Published online 30 June 2012 *Nucleic Acids Research, 2012, Vol. 40, No. 17* ***8743–8758***
doi:10.1093/nar/gks633

Crystal structure of the UvrB dimer: insights into the nature and functioning of the UvrAB damage engagement and UvrB–DNA complexes

Matthew P. J. Webster[1,2], Rachael Jukes[3], Vlad S. Zamfir[4], Christopher W. M. Kay[4,5], Claire Bagnéris[1] and Tracey Barrett[1,*]

[1]Department of Biological Sciences, Institute of Structural and Molecular Biology, Crystallography, Birkbeck College, Malet Street, London WC1E 7HX, [2]Macromolecular Structure and function Laboratory, Cancer Research UK London Research Institute, Lincoln's Inn Fields Laboratories, 44 Lincoln's Inns Fields, London WC2A 3LY, [3]Cancer Research UK DNA Repair Enzymes Group, Genome damage and stability Centre, School of Life Sciences, University of Sussex, Falmer, Brighton BN1 9QJ, [4]Department of Structural Molecular Biology, Institute of Structural and Molecular Biology, UCL, London WC1E 6BT and [5]London Centre for Nanotechnology, University College London, 17-19 Gordon Street, London WC1H 0AH, UK

Received December 15, 2011; Revised May 31, 2012; Accepted June 4, 2012

ABSTRACT

UvrB has a central role in the highly conserved UvrABC pathway functioning not only as a damage recognition element but also as an essential component of the lesion tracking machinery. While it has been recently confirmed that the tracking assembly comprises a $UvrA_2B_2$ heterotetramer, the configurations of the damage engagement and UvrB–DNA handover complexes remain obscure. Here, we present the first crystal structure of a UvrB dimer whose biological significance has been verified using both chemical cross-linking and electron paramagnetic resonance spectroscopy. We demonstrate that this dimeric species stably associates with UvrA and forms a $UvrA_2B_2$–DNA complex. Our studies also illustrate how signals are transduced between the ATP and DNA binding sites to generate the helicase activity pivotal to handover and formation of the $UvrB_2$–DNA complex, providing key insights into the configurations of these important repair intermediates.

INTRODUCTION

Nucleotide excision repair is a highly conserved mechanism that efficiently corrects bulky DNA adducts. These lesions arise from exposure to endogenous/exogenous agents and are targeted by the UvrABC pathway in bacteria. This mechanism utilizes three core proteins; UvrA, B and C that act co-operatively to form tracking, damage detection and incision complexes (1,2). Formation of the tracking complex involves assembly of a UvrAB intermediate (3) which has the ability to locate sites of potential damage typified by local DNA distortions, and is largely driven by the limited helicase activity of UvrB (4). Once a lesion has been identified, the UvrAB complex undergoes a substantial conformational change in which the DNA becomes partially unwound in close proximity to the adduct and wrapped around UvrB (5,6). The result is complete transfer of the duplex to UvrB (subsequently termed 'handover') and the formation of a tight UvrB–DNA complex that is thought to promote dissociation of UvrA and formation of the pre-incision complex. This is followed by the recruitment of UvrC, via UvrB–UvrC interactions mediated by a mutually conserved helix-loop-helix motif (domain 4 in UvrB), which catalyses dual incisions ~5 nt 3′ and ~8 nt 5′ to the lesion (1,7–9). UvrC and the incised fragment are then released from the highly stable BC–DNA complex by the helicase UvrD and UvrB displaced by DNA polymerase I that utilizes the resultant gapped duplex as a template for resynthesis (10,11). Repair is concluded by restoration of the covalent continuity by DNA ligase.

There has been significant debate regarding the multimerization state of UvrB in solution (8,12–14), where it has been proposed that a dimer functions as part of the UvrAB damage location complex (15,16). This controversy is largely due to conflicting biochemical/biophysical data where it remains to be unequivocally established whether the pre-incision complex involves a UvrB monomer or dimer. The stoichiometry of UvrB in the tracking assembly, however, which functions as a $UvrA_2B_2$ heterotetramer, has recently been confirmed by the

*To whom correspondence should be addressed. Tel: +44 207 631 6822; Fax: +44 207 631 6803; Email: t.barrett@mail.cryst.bbk.ac.uk

structural studies of Pakotiprapha *et al.* (17). Interestingly, the two UvrB monomers in the reported crystal structure are positioned ~145 Å apart and are each ~80 Å from the proposed lesion site. These findings are consistent with a sub-optimal arrangement for handover as suggested by the authors. In our initial efforts to further investigate the nature of UvrB's limited helicase activity, pivotal to lesion detection and formation of the pre-incision complex, we by chance crystallized a UvrB dimer in complex with ssDNA and the non-hydrolysable ATP analogue AMPPCP that was subsequently refined to 3.25 Å. In addition to deducing how signals are transduced between the ATP and DNA binding sites, we were able to verify that this dimer is physiological and demonstrate that it not only interacts with UvrA, but also forms a tight $UvrA_2B_2$–DNA complex in addition to a stable $UvrB_2$–DNA complex on a self-loading substrate. These findings lead us to investigate the nature of these complexes using a combination of molecular modeling and site directed mutagenesis/biochemical assays. Our studies have suggested a mode of association between our dimer and UvrA in which all of the key elements are more favourably aligned in closer proximity to the lesion than observed in the recently reported $UvrA_2B_2$ complex and reveal that the helicase activity of UvrB drives relative motions between the two monomers for engagement with the duplex. We were also able to generate a model of the $UvrB_2$–DNA 'handover' complex that predicted the direct participation of domain 2 in DNA binding (previously assigned the exclusive role of interacting with UvrA) that we were subsequently able to verify. Taken together, our results indicate that the UvrB dimer complex is mimetic of both the damage engagement and UvrB–DNA complexes.

MATERIALS AND METHODS

Protein purification and mutagenesis

Bacillus subtillis UvrB was expressed and purified as previously described (18). All mutants were generated using the Quick-change mutagenesis kit (Agilent Technologies) and were expressed/purified using the protocol reported for the native protein. For the expression of UvrA, a pET8c vector containing the *B. subtilis* UvrA insert (gift from Bernard Connolly, University of Newcastle) was transformed into BL21 DE3 pLysS cells (Invitrogen) and grown at 37°C in LB medium supplemented with 100 μM Ampicillin and 100 μM Chloramphenicol until an OD_{600nm} of 0.6 was reached. The temperature was then reduced to 20°C and the cultures were induced with 1 mM IPTG overnight. Cells were harvested by centrifugation and the resulting pellet resuspended in Buffer A (50 mM Tris–HCl (pH 7.4), 300 mM NaCl, 20% Glycerol, 0.01% Tween (Sigma), 2 mM TCEP-HCl (Roche) and 10 mM Imidazole). They were subsequently lysed by sonication on ice in the presence of an EDTA-free protease inhibitor cocktail tablet (Roche). Lysates were clarified by further centrifugation at 20 000 rpm for 60 min. The resultant supernatant was loaded onto a 10 ml Talon column (GE Healthcare) and washed with 10 column volumes (CVs) of Buffer A. UvrA was eluted using a gradient of 0–100% Buffer B (50 mM Tris–HCl (pH 7.4), 300 mM NaCl, 20% Glycerol, 0.01% Tween (Sigma), 2 mM TCEP-HCl (Roche) and 500 mM Imidazole) over 10 CV. Purification to homogeneity was achieved using size exclusion chromatography where UvrA fractions from the Talon purification step were loaded onto a 300 ml S-200 Gel Filtration column, pre-equilibrated with a buffer comprising 50 mM Tris–HCl (pH 7.4), 300 mM NaCl, 20% Glycerol, 0.01% Tween (Sigma) and 2 mM TCEP-HCl (Roche). The resulting fractions were then analysed using SDS–PAGE and those with a purity of greater than 95% pooled and stored at −80°C.

Chemical cross-linking and dimer purification

Chemical cross-linking was performed using the homobifunctional cross-linking agent 1,8-bis-maleimidodiethyleneglycol ($BM(PEG)_2$, Thermo scientific) and the T481C mutant following the manufacturer's directions. Cross-linked T481C UvrB ($UvrB_2X$) was separated from non-adducted proteins by gel filtration using a 300 ml S-200 column equilibrated in a buffer comprising 50 mM Tris–HCl (pH 7.4), 500 mM NaCl and 5% glycerol.

EPR spectroscopy

The T481C mutant was spin labeled using the cysteine specific nitroxide spin label 3-(2-iodoacetamido)-proxyl (PROXYL). In order to maximize labeling efficiency, the mutant, purified up to the talon stage, (18) was dialyzed overnight in talon buffer A (50 mM Tris–HCl, pH 7.4, 300 mM NaCl) supplemented with 5 mM dithiothreitol (DTT) to ensure that C481 was fully reduced. This was followed by a buffer exchange step using a GE Healthcare Hi-prep 26/60 de-salting column (pre-equilibrated with talon buffer A) to remove the DTT prior to overnight incubation with a 20-fold excess of PROXYL. The labeled mutant was subsequently purified using gel filtration on a 300 ml S-75 column that had been equilibrated in a buffer comprising 50 mM Tris–HCl, pH 7.4, 300 mM NaCl and 10% glycerol. The various fractions were then analysed using SDS–PAGE and those containing UvrB at a purity of greater than 95% pooled and concentrated. Wild-type UvrB was labeled using the identical protocol and both proteins analysed as detailed below.

Continuous-wave electron paramagnetic resonance (cw-EPR) experiments were performed at room temperature on the labeled T481C mutant (at 104 μM) and wild-type UvrB (at 100 μM) on a Bruker EMXplus spectrometer operating at 9.4 GHz equipped with a 4122SHQE resonator. Measurements were performed using 0.2 mW microwave power, 100 kHz modulation frequency, 0.1 mT modulation amplitude and 10 ms conversion time and time constant. Four pulse double electron–electron resonance (DEER) experiments (19) were performed at 50 K on a Bruker ELEXSYS E580 spectrometer operating at 9.6 GHz equipped with an ER-4118-X-MD-5 resonator, Oxford Instruments continuous flow cryostat (CF935) and ITC503 temperature controller. Distance distributions were extracted from the resulting

spectra using the programme DeerAnalysis2011 running in a Matlab™ environment (20).

Gel-shift assays

DNA duplexes used in the gel shift assays are shown in Table 1. NB. * denotes a fluorescein adducted thymine base.

For the UvrB self-loading assays, 2.7 μM UvrB (or $UvrB_2X$) was incubated with 200 nM G10 in binding buffer (20 mM Tris–HCl (pH 7.6), 50 mM NaCl, 4% Ficoll, 10 mM $MgCl_2$ and 10 mM ATP) for 30 min at 25°C before loading onto a pre-cast 6% PAGE gel (Invitrogen). Following loading, the gels were run on ice for 90 min in 1× TBE buffer at 100 V. Handover assays were performed with the T50 substrate and conducted in an identical manner but with the addition of 0.45 μM UvrA. All gels were visualized using a UV transilluminator to detect the intrinsic fluorescence of the fluorescein moiety.

The capacity of cross-linked UvrB and generated mutants to associate with UvrA was assessed by non-denaturing PAGE using the Novex® Bis-Tris Gel System (Invitrogen). UvrA and UvrB at 2.5 μM concentration were incubated in a buffer comprising 20 mM Tris–HCl (pH 7.5), 150 mM KCl, 5% Glycerol, 5 mM β-Mercaptoethanol, 5 mM $MgCl_2$ and 2 mM ATP at 25°C for 30 min. Following loading, the gels were run on ice for 60 min at 150 V followed by 60 min at 250 V using the supplied buffers.

ATPase assays

The conversion of ATP to ADP by UvrA and UvrB was determined using a steady-state coupled enzyme assay system consisting of pyruvate kinase and lactate dehydrogenase that linked ATP hydrolysis to the oxidation of NADH. Assays were performed in a buffer consisting of 50 mM Tris–HCl (pH 7.5), 50 mM NaCl, 4 mM $MgCl_2$, 1 mM DTT, 20 U/ml lactate dehydrogenase, 20 U/ml pyruvate kinase, 2 mM phosphoenol pyruvate, 0.15 mM NADH, 1 mM ATP to which 50 nM UvrA and/or UvrB ($UvrB_2X$ or T481C mutant) was added in the presence or absence of 5 μM ssDNA (sequence GGCTGCCTGCGC). The change in absorbance was monitored at 340 nm using a Cary UV spectrophotometer at 25°C. Turnover rates were determined by linear regression using the Cary UV spectrophotometer software.

Crystallization, data collection and structure determination

Protein DNA complexes were generated by incubating UvrB with the oligonucleotide 5′-TACTG(TF6)TT-3′ (where TF6 is T-fluorescein) in a protein:DNA ratio of 1:1.2. The non-hydrolysable ATP analogue AMPPCP (Invitrogen) was then added to a final concentration of 10 mM. The resultant solution was concentrated to 10 mg/ml (UvrB concentration) and used to set up microbatch crystallization trials at 16°C. Crystals of the UvrB–DNA–AMPPCP complex grew within a few days in the conditions 0.1 M MES pH 6.5, 12% PEG 20 000. They were subsequently cryo-protected in 20% glycerol and flash frozen in liquid nitrogen.

Data were collected on beamline ID23-2 at the ESRF on a single flash frozen crystal to 3.25 Å that were then integrated and scaled using the programs XDS (21) and XSCALE (22). The structure was solved by molecular replacement using PHASER (23), manually re-built in COOT (24) and refined using PHENIX where NCS restraints and TLS refinement were first introduced (25). This was followed by subsequent cycles of re-building and refinement in AUTOBUSTER (26). The final model comprises two UvrB monomers (excluding domain 4 for which no density could be identified), seven nucleotides from each of the DNA 8mers and two partially ordered AMPPCP molecules. All geometric parameters are well within the expected ranges for a structure at this resolution (Table 2). The co-ordinates and structure factors have been deposited in the protein data bank under the accession code 3V4R.

Table 1. Duplexes used in the gel shift and handover assays

G10	5′-TACTTACGGCCACATTACTAC*GGAACTCAGAACGAGCTG-3′
	3′-AATGATGACCTTGAGTCTTGCTCGAC-5′
T50	5′-GACTGTACTTACGGCCACATTACTAC*GGAACTCAGAACGAGCT GATCGC-3′
	3′-CTGACATGAATGCCGGTGTAATGATGACCTTGAGTCTTGCTCG ACTAGCG-5′

RESULTS

Overall dimer structure, DNA and ATP binding sites

Preliminary analysis of the diffraction data suggested that UvrB had crystallized as a dimer and was later verified by molecular replacement where the protein co-ordinates from the UvrB trithymine ternary complex (2D7D.pdb) were used as a search model that yielded two solutions. Analysis of the structure revealed that the two UvrB monomers (subsequently referred to as monomer A and monomer B) were related by an NCS 2-fold axis resulting in a 'head-to-head' relative orientation (Figure 1A). Both monomers were highly similar having an RMSD of ~0.8 Å when superposed (calculated using all atoms in the residue range 1–587). Electron density for nucleotides 2–7 of both strands was observed and although density for the AMPPCP molecule associated with monomer A could be identified (excluding the γ phosphate), only the α and β phosphates were ordered for the molecule associated with monomer B. Despite these differences, the overall configurations of the two ATP binding sites are largely identical and very similar to those reported in the ADP–DNA–UvrB monomeric structures (Supplementary Figure S1A). It was therefore unlikely that formation of the dimer could be attributed to non-physiological conformational changes induced or mediated by use of the non-hydrolysable ATP analogue AMPPCP as confirmed by chemical cross-linking and EPR spectroscopy (see below). No ordered density could be identified for the T-fluorescein moieties in either of the DNA 8mers.

There are several notable differences between the DNA in our dimer and the reported UvrB-DNA structures. Although nucleotides T5 and T6 adopt similar positions

Table 2. Data Collection and Refinement Statistics

Space group	$P2_12_12_1$
Unit cell [a,b,c (Å)]	95.94 100.31 163.63
Resolution (Å)	20.0 3.25 (3.33–3.25)[a]
Total no. of reflections	185 384
No. of unique reflections	25 439
Redundancy	7.3 (7.5)
Completeness (%)	99.4 (100.0)
$<I>/<\sigma(I)>$	9.3 (3.2)
R_{merge}[b] (%)	14.9 (76.1)
Refinement	
No. of protein atoms	8532
No. of DNA atoms	254
No. of AMPPCP atoms	35
R_{cryst}[c]/R_{free}[d] (%)	18.0/21.9
Luzzati plot co-ordinate error (Å)	0.52
Overall B-factors (Å^2)[e]	68.8/68.4/83.7/113
Deviations from ideal stereochemistry	
RMSD bonds (Å)	0.01
RMSD angles (°)	1.22
Wilson B-factor (Å^2)	89.4
Ramachandran plot analysis[f]	
Most favoured (%)	95.00
Additionally allowed (%)	3.44
Disallowed (%)	1.56

[a]Values in parentheses are for the highest resolution shell (3.33–3.25 Å).
[b]$R_{merge} = \Sigma(|I_i - <I>|)/\Sigma(<I>)$, where the sum is calculated over all observations of a measured reflection (I_i), and $<I>$ is the mean intensity of all the measured observations (I_i).
[c]$R_{cryst} = \Sigma\ (|F_{obs} - F_{calc}|)/\Sigma\ (F_{obs})$, F_{obs} are the observed structure factor amplitudes and F_{calc} those calculated from the model.
[d]R_{free} is equivalent to R_{cryst} but where 5% of the measured reflections have been excluded from refinement and set aside for cross-validation purposes.
[e]Average B-values for all atoms/protein/DNA/AMPPCP/.
[f]Ramachandran plot analysis was from Molprobity (27).

to their analogues in these complexes, A2-T3 extend across the gap between domains 1a and 3 similar to the protein–DNA complexes of PcrA and other SF1/SF2 helicases where these domains are conserved (28) (Figure 1B). In contrast to these structures, however, very few specific contacts are mediated by domain 3. They are exclusively limited to a stacking interaction between the aromatic moiety of Phe527 and the adenine base of A2 together with a single hydrogen bond donated by the guanadinium group of Arg506 to O2P of C3 in monomer B (Figure 1C and Supplementary Figure S1B). Phe527, although a non-essential residue, has been proposed to intercalate into the damaged duplex in order to generate an appropriate substrate for UvrC cleavage (1). Conversely, site directed mutagenesis has shown Arg506 to be an important residue for handover and formation of the pre-incision complex (29) that in our structure also interacts with the carbonyl oxygen of Ser477 directly adjacent to Glu478. Glu478 is a key residue for UvrC incision implicated in DNA remodeling (30,31) (Figure 1C). Interestingly, Arg506 is connected to the ATP binding site via a network of salt bridges and hydrogen bonds (Figure 2A). These are mediated by Arg540 (that contacts the carbonyl oxygen of Arg506), and Asp510 whose carboxylate group is 'sandwiched' between the guanadinium moieties of Arg540 and Arg543, that is critical for ATP binding. All of these residues are either important or essential for repair and when mutated result in a similar phenotype of attenuated ATP, DNA binding and handover activities consistent with their pivotal involvement in coupling ATP hydrolysis to DNA binding (29,32).

Our complex reveals that T7, located behind the β-hairpin motif in domain 1a, is extra-helical in the strand associated with monomer A but intra-helical in that bound to monomer B (subsequently denoted as intraS and extraS, respectively; Figure 2B). Although no major re-arrangements are evident, a slight relative shift between the two strands (Figure 2C) places the furanose ring of TF6 in extraS, closer to the β-hairpin. This would result in minor steric clashes with the analogous ring of T7 if in the intra-helical position adopted in intraS, suggesting that steric factors have a role in the conformational switch. Interestingly, base flipping has also been observed in the UvrB–stem loop structure (2FDC.pdb), however, the nucleotide concerned is located directly 5′ to T7 and is thus in a non-equivalent position (Supplementary Figure S1C). Rather than stacking against the aromatic moiety of Phe249, a non-essential residue, the 'flipped' thymine base in our dimer is located in a recess formed by residues Gly147–Gly149 and His248–Val250 (disordered in monomer B; Figure 2B and Supplementary Figure S1C). These residues contact T7 via a plethora of van der Waals interactions and would favourably accommodate guanine, adenine or cytosine. T7 is further stabilized by hydrogen bonds donated by the guanidinium head group of Arg123 (essential for handover) (33) and the NH moiety of Gly149 to the exocyclic oxygen atoms O2 and O4. Interestingly, Phe249 occludes this recess in the stem loop structure as a result of substantial re-modeling of the His248–Val250 loop that becomes apparent when the two structures are superposed (Supplementary Figure S1C). These re-arrangements are in response to the re-positioning of domain 2 in our dimer relative to the monomeric UvrB structures (see below).

The dimer interface

Three regions of contact form the dimer interface that encompasses the β-hairpin, elements from domain 2 and the helix spanning amino acids Ser481–Lys495 at the periphery of domain 3, all of which are highly conserved (Figure 3A–C and Supplementary Figure S2A). While the β-hairpin functions in DNA binding and lesion detection, domain 2 is the association site for UvrA (1,13). Domain 3 is also essential for repair as it forms one half of the ATP binding site (32). Analysis of the dimer interface reveals a lack of extensive contacts with those observed being largely electrostatic or van der Waals interactions. This absence of extensive contacts is illustrated by the burial of only ~1276 Å^2 of accessible surface area (compared to ~4300 Å^2 in the *B. stearothermophilus* UvrA dimer). The most striking of the interfacial interactions involves the β-hairpin and domain 2. Remarkably, domain 2 undergoes a rigid body rotation of ~30° relative to its position in the trithymine complex (and the other monomeric UvrB structures in which domain 2 is visible; Figure 3A and Supplementary Figure S2B), coupled with

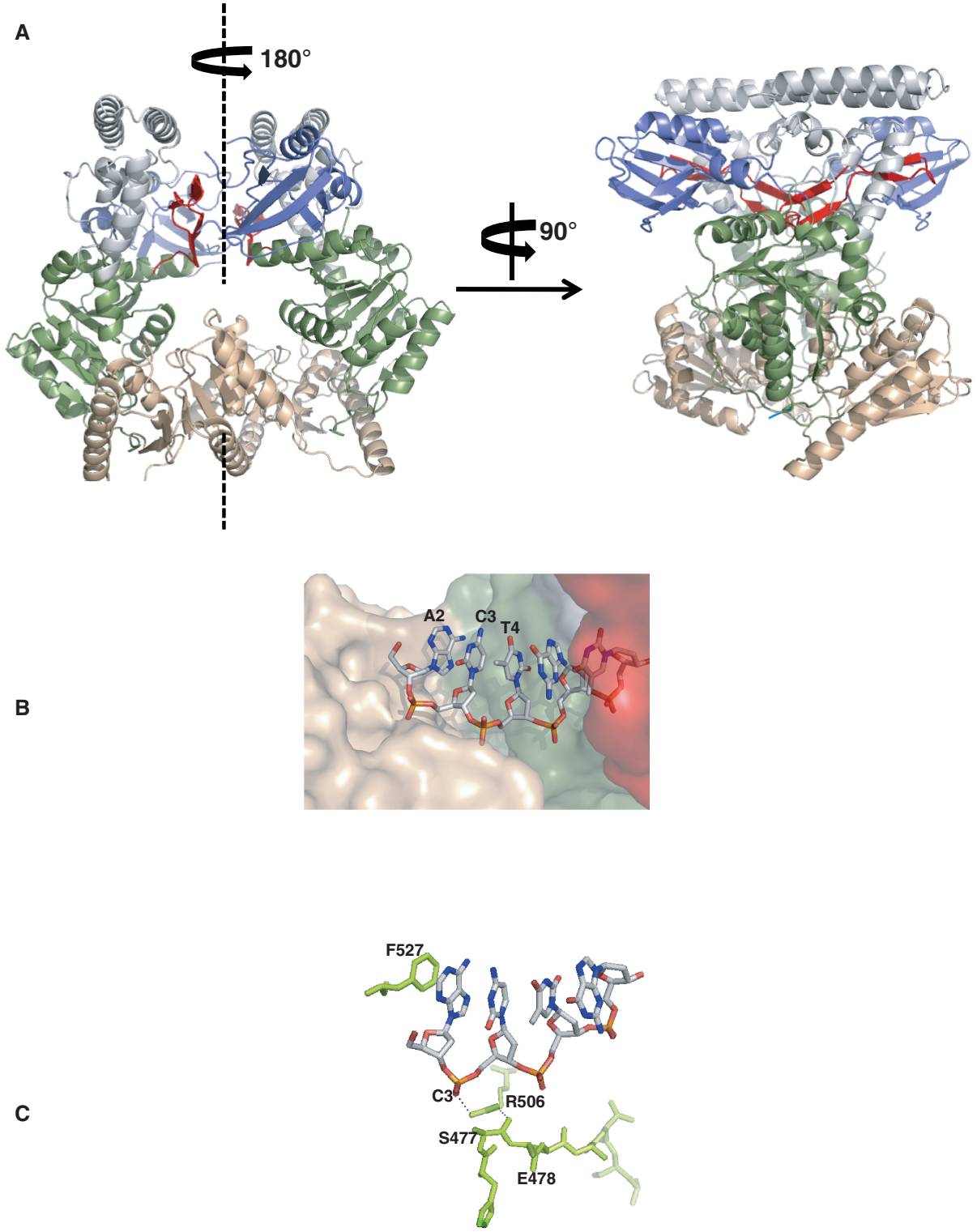

Figure 1. (**A**) Cartoon of the UvrB dimer with domains 1a, 1b, 2, 3 and the β-hairpin highlighted in green, grey, blue, light brown and red, respectively. (**B**) View of nucleotides A2 to T4 (sticks) associated with monomer A (depicted as van der Waals spheres) that extend across the domain 1a-domain 3 interface (coloured as above) similar to the analogous nucleotides in monomer B. (**C**) The domain 3–DNA interactions (domain 3 is shown in green). Arg506 donates a hydrogen bond to O2P of C3, while also donating a hydrogen bond to the carbonyl oxygen of Ser477. A2 is stabilized by a stacking interaction involving Phe527.

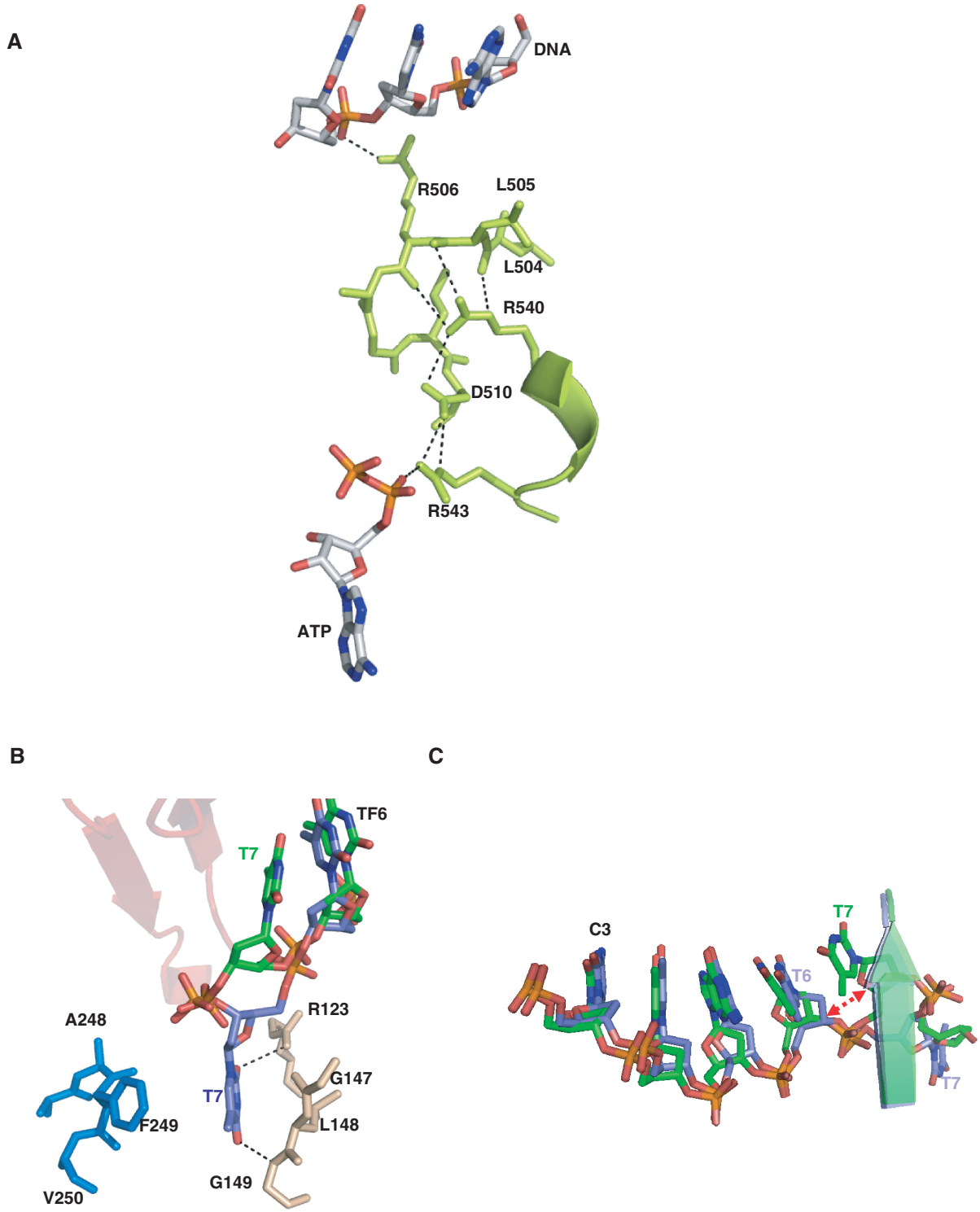

Figure 2. (**A**) Arg506 directly connects the DNA and ATP binding sites via a network of hydrogen bonds and salt bridges. This involves Arg540, Asp510 and Arg543; all of which are essential for repair. (**B**) T7 is extra-helical in monomer A (slate), but intra-helical in monomer B (green). The extra-helical thymine is stabilized in a recess formed by residues Val250, Phe249 and Ala248 in domain 2 and Gly147, Leu148 and Gly149 in domain 1a that contribute largely van der Waals contacts. The exocyclic oxygens are stabilized by the guanadinium group of Arg123 (also in domain 1a) and the main chain NH group of Gly149. All domains are coloured as above. (**C**) Superposition of nucleotides C3 to T7 in monomer A (extraS, slate) and monomer B (intraS, green). A slight translocation of extraS towards the β-hairpin could potentially disfavour the intra-helical conformation of T7 present in intraS as a result of steric clashes between the furanose rings of T6 and T7 (red arrow).

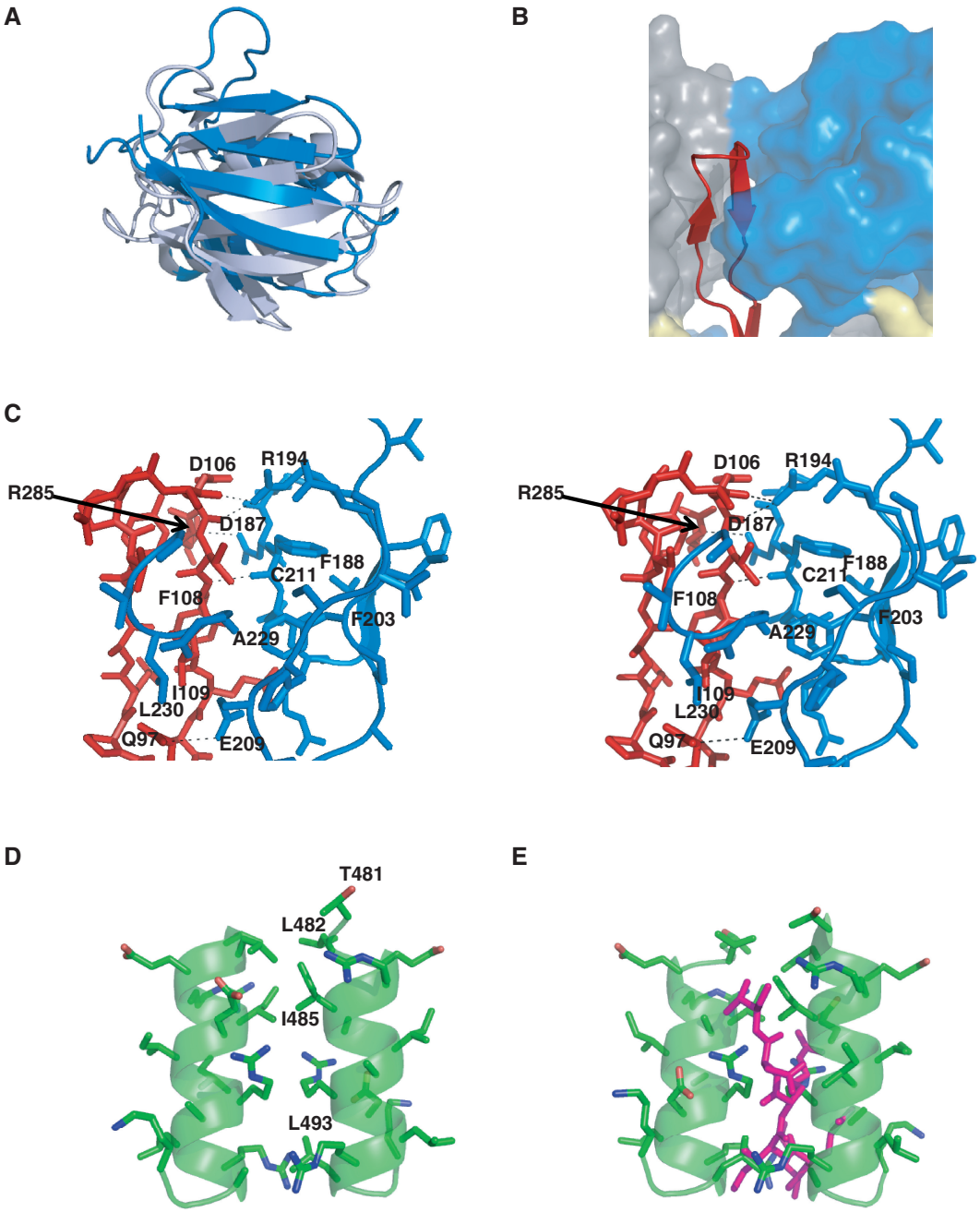

Figure 3. (**A**) Superposition of domain 2 from monomer B with domain 2 from the trithymine UvrB–DNA complex (2D7D.pdb) reveals considerable re-modeling and a relative rotation of ~30°. (**B**) The re-configuration of domain 2 in each monomer gives rise to partial encapsulation of the β-hairpin motifs that (**C**) mediate a range of electrostatic, van der Waals and hydrophobic interactions. These include hydrogen bonds donated by the guanadinium group of Arg194 (domain 2) to the carbonyl oxygens of Asp106 and Thr105, respectively (β-hairpin), the amide nitrogen of Gln97 (β-hairpin) to the carboxylate group of Glu209 (domain 2) and the carboxylate group of Asp187 to the guanadinium moiety of Arg285. This configuration of the β-hairpin and domain 2 is further stabilized by hydrophobic interactions involving Thr107, Ile109, Val102 (β-hairpin) and Phe203, Cys211, Ala229 and Leu230 (domain 2). (**D**) The domain 3 dimer interface comprises the highly conserved helix spanning residues Ser481–Lys495 and is largely mixed where Thr481, Leu482, Ile485, Leu493 contribute hydrophobic interactions. (**E**) Superposition of the domain 3 interface with the *B. caldotenax* UvrB co-ordinates (1D9X.pdb) reveals that the C-terminal residues (magenta) in the wild-type monomer would prevent full dimerization of UvrB consistent with their proposed auto inhibitory role.

major remodeling of residues Val227–Asp239 and Phe244–Thr251 located towards the C-terminus of the domain. These changes result in partial encapsulation of the β-hairpin tip in the NCS related monomer that additionally promotes favourable interactions with residues at the hairpin base (Figure 3B and C). In this configuration, residues Asp106–Gln110 at the C-terminus of the β-hairpin form a plethora of interactions with residues comprising the central β-sheet of domain 2. These include hydrogen bonds donated by the guanadinium

head group of Arg194 in domain 2 to the carbonyl oxygens of Asp106 and Thr105 at the hairpin tip, respectively (Figure 3C). In addition, the carbonyl oxygen of Phe108 receives a hydrogen bond from the peptide NH group of Phe188 whose aromatic side chain contributes to a largely hydrophobic cavity created by Thr107, Ile109, Val102 (β-hairpin) and Phe203, Cys211, Ala229 and Leu230 (domain 2). Towards the hairpin base, the amide NH group of Gln97 donates a hydrogen bond to the carboxylate group of Glu209. In addition, Asp187 receives a hydrogen bond from Arg285 in the β-hairpin-domain 1b interface. Residues Ile186–Gln189 of domain 2 also participates in a series of van der Waals interactions involving residues Asp106–Phe108 located at the β-hairpin tip. Mutagenesis studies have shown that residues at the hairpin tip are essential for the handover of DNA from UvrA to UvrB and for damage recognition (1).

The composition of the interface contributed by domain 3 though mixed in terms of amino acid type, consists almost entirely of van der Waals interactions with the exception of hydrophobic contacts contributed by Leu482, Ile485 and Leu493 (Figure 3D). Unlike the previous monomeric *B. caldotenax* UvrB structures, there is no visible density beyond residues Thr590 and Asn589 in monomers A and B, respectively. Interestingly, residues Lys590–Val595 in these monomeric structures occupy the position of the domain 3 interface observed in our complex and would thus disfavour dimerization (Figure 3E). Interestingly, these residues are also absent in the monomeric *B. subtilis* DNA–ADP ternary complexes where their presence in positions analogous to those in the *B. caldotenax* structures would prevent the close approach of domains 1a and 3 required for completion of an active ATP binding site proposed by Eryilmaz *et al.* (18). Our findings are thus consistent with the auto inhibitory role proposed for the C-terminal region of UvrB (18,34) whose dimerization has been suggested to prevent the premature recruitment of UvrC prior to UvrB's proper engagement with a lesion (15).

Verification of the UvrB dimer

Although the localization of functionally important residues to the dimer interface was circumstantially suggestive of a biologically relevant assembly, we were able to confirm this using chemical cross-linking and EPR spectroscopy. We initially targeted domain 3 to minimize the potential impact on DNA and ATP binding. Coincidentally, T481, a non-essential residue (data not shown) positioned at the periphery of the dimer interface, is located a distance of 14.9 Å from its NCS related partner (measured from OG1 atoms; Figure 4A) that matches almost exactly the 14.7 Å linker length of the sulphydryl cross-linking reagent (BM)PEG_2, designed to specifically react with cysteine residues. A T481C mutant was therefore generated as a potential cross-linking site. This substitution was shown to have little effect on UvrB's affinity for the G10 duplex (Table 1 and Figure 4B), and the mutant was subsequently found to be proficient in handover (Supplementary Figure S3A). Cross-linking of the T481C mutant with (BM)PEG_2 resulted in a shift from a monomeric to a dimeric species on SDS–PAGE gels while the native protein remained monomeric following identical treatment (Figure 4C). Non-specific association could be discounted since control experiments in which cross-linking was performed in the presence of Grb2 (an SH2 domain protein), which contains a single reactive cysteine, showed no evidence of a UvrB-Grb2 heterodimer (Supplementary Figure S3B).

To independently confirm that the UvrB dimer observed in our crystal structure exists in solution, we modified the T481C mutant with a nitroxide spin label for EPR studies in order to ascertain whether a distance consistent with the ~15 Å observed in our complex, measured between the C481 SG atoms, could be identified (see 'Materials and Methods' section). Despite the wild type (WT) protein containing three endogenous cysteines (Cys144, Cys211 and Cys303) cw-EPR spectra, obtained at room temperature, exhibited low signal intensity (Figure 5A), indicating poor accessibility for labeling as expected from the crystal structure. In contrast, the T481C mutant showed an 18-fold relative increase in EPR signal demonstrating that this solvent-exposed position had been successfully spin-labeled. DEER spectroscopy was performed on the T481C mutant to determine the distance between the dimer-related C481 residues. The distance distribution (Figure 5B), obtained by Tikhonov regularization of the dipolar evolution following baseline correction of the raw data (Supplementary Figure S3C and D), has a maximum at ~17 Å. Given that this distance is measured between spin labels that are naturally further apart, it is entirely consistent with the 15 Å observed in our crystal structure (Figure 5B). This short distance, therefore, can be unambiguously attributed to the dimer related C481 residues. Although longer distances are also evident, they are likely to be those between C481 and the small fraction of labeled endogenous cysteines. The 18-fold reduction in EPR signal meant, however, that it was not possible to obtain reliable distance data for the WT protein. These results therefore corroborate the physiological relevance of our dimer in keeping with the mechanistic importance of the motifs involved.

$UvrB_2X$ interacts with UvrA and forms a trapped $UvrA_2B_2$ complex on DNA

We next investigated whether our observed dimer could interact with UvrA. Structural and site-directed mutagenesis studies have confirmed that residues Arg183, Arg198 (and to a lesser extent Glu215 and Arg223) mediate crucial interactions with UvrA (13). In the context of our dimer, these map to a largely solvent exposed surface. Using the co-ordinates of the UvrA (insertion domain)–UvrB (domain 2) structure (3FPN.pdb), we were able to successfully dock the UvrA interaction domain onto each of the UvrB domain 2 monomers in our complex (via domain 2 superposition) with no major steric clashes (Figure 5C). This prompted us to establish whether $UvrB_2X$, purified to homogeneity using gel filtration (see 'Materials and Methods' section), could associate with UvrA in solution using native PAGE. Our results show that this dimeric

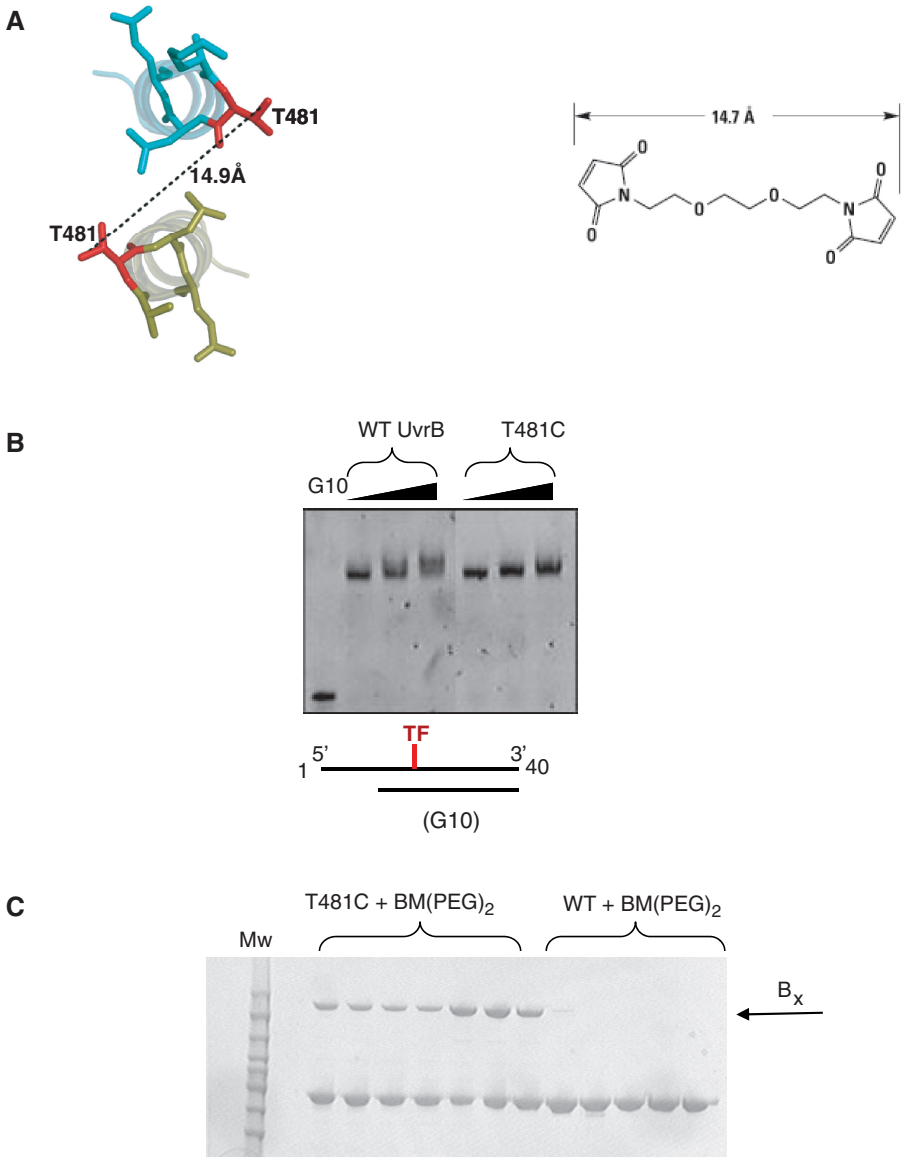

Figure 4. (**A**) Left panel: the relative positions of the NCS related T481 residues whose OG1 atoms are separated by 14.9 Å, consistent with the cross-linking agent $BM(PEG)_2$. Right panel: the structure of $BM(PEG)_2$. (**B**) Gel shift assay of the T481C mutant using the G10 duplex. The T481C mutant has comparable binding activity to wild-type UvrB. (**C**) SDS–PAGE gel of WT UvrB and the T481C mutant after treatment with the cross-linking agent $BM(PEG)_2$.

species does indeed interact with UvrA where the resulting complex co-elutes with that observed for WT UvrB (Figure 6A). We also investigated whether $UvrB_2X$ could form a $UvrA_2B_2$ complex on DNA using a gel shift assay. While incubation of WT UvrB with UvrA, T-fluorescein adducted DNA and ATP resulted in formation of a UvrAB–DNA and a UvrB–DNA complex as a result of handover, the same experiment conducted with $UvrB_2X$ showed only the presence of a $UvrA_2B_2X$–DNA band (Figure 6B). The $UvrA_2B_2X$ complex was therefore completely defective in handover and trapped on the DNA. To ascertain whether this might be attributable to attenuated DNA binding activity, gel shift assays were performed using $UvrB_2X$ and the G10 duplex. These studies revealed near wild-type binding affinity thus excluding this possibility (Figure 6C), although the shifted species in the $UvrB_2X$–DNA complex has slightly reduced mobility relative to that of the wild-type dimer; possibly due to increased bending of the DNA caused by strain induced by the cross-linker. It has been shown that handover is dependent on the 'cryptic' ATPase activity of UvrB that becomes unmasked in the presence of DNA and UvrA (4). Mutagenesis studies targeting K45 in the Walker B motif of the ATP binding site resulted in a similar phenomenon to what we observe where the $UvrA_2B_2$ mutant complex remains trapped on the DNA (15). This mutant has been proposed to promote dimerization of UvrB within the complex due to its inability to hydrolyse ATP to ADP that has a destabilizing effect. Interestingly, ATPase assays of $UvrB_2X$ showed

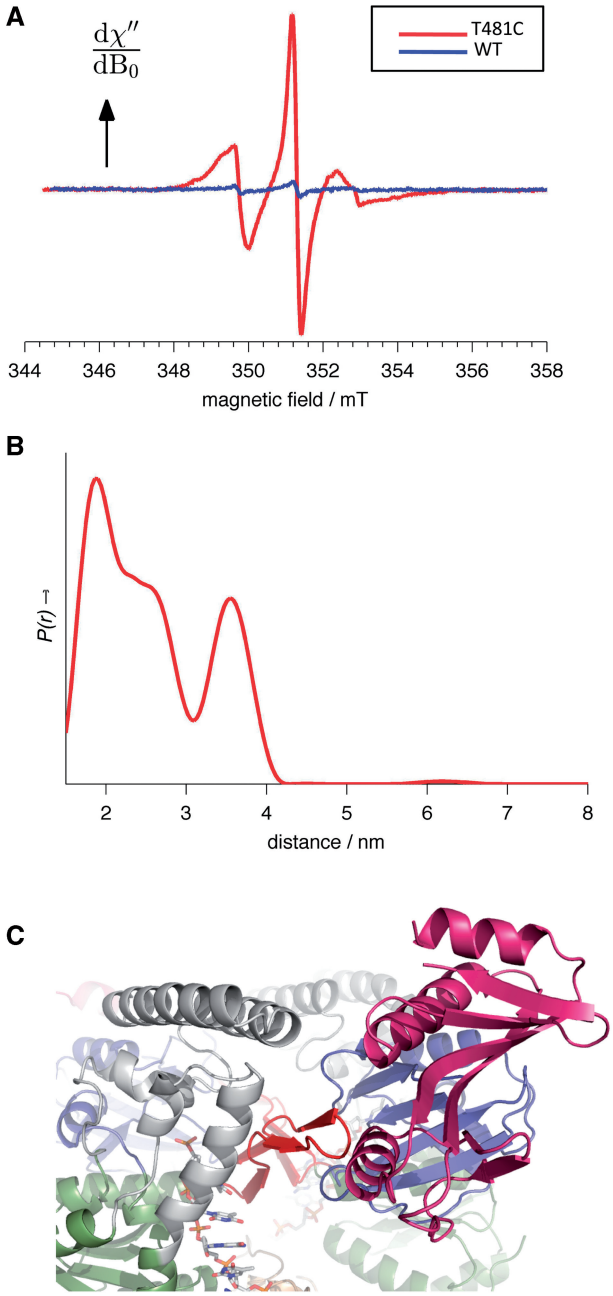

Figure 5. (**A**) Cw-EPR spectra of WT UvrB (blue) and the T481C mutant (red) recorded at room temperature. (**B**) Distance distribution obtained by Tikhonov regularization of the 4 pulse DEER spectrum (Supplementary Figure S3D). (**C**) Docking of the UvrA UvrB interacting domain (magenta) onto the UvrB dimer (via superposition of the domain 2 residues in the UvrA(interacting domain)–UvrB(interacting domain) complex (3FPN.pdb) results in no major steric clashes.

that while the basal level of ATP turnover was reduced only ~2.5-fold relative to native UvrB, it could no longer be stimulated by ssDNA (Figure 6D). This is in contrast to the T481C mutant that had a higher basal rate of ATP hydrolysis, but was stimulated to levels comparable to those observed for wild-type UvrB. Our results therefore suggest that the observed handover defect originates from the inability of $UvrB_2X$ to efficiently couple ATP hydrolysis to DNA binding required to drive relative motions between the two monomers for duplex loading.

Putative models of the $UvrA_2B_2$–DNA and $UvrB_2$–DNA complexes

Given that UvrA was able to interact favourably with $UvrB_2X$, we next sought to probe the nature of this association. Initially, docking studies were performed using the available structures of UvrA and the recently reported $UvrA_2B_2$ complex. All attempts to superpose each of the monomers in our dimer with their analogues in the $UvrA_2B_2$ complex resulted in major steric clashes with the insertion domains and signature II motifs of UvrA. The UvrB binding domain of UvrA has, however, been shown to have high conformational flexibility based on the available UvrA structures where an unprecedented rotation of ~90° towards the dimer interface, along with re-arrangement of the insertion domains, is observed in the *Mycobacterium tuberculosis* homologue (35). In keeping with this, an intermediate configuration in which the UvrB binding domains undergo a more modest rotation of ~30° appeared to interact favourably with both monomers (Figure 6E). In this position, the NCS 2-fold axes relating the UvrA and UvrB monomers are aligned and the tip of the β-hairpin of each UvrB molecule is brought into close proximity to UvrA's UvrB binding domain. This brings the N-terminus of the helix spanning amino acids 257–277 in domain 1b that encompasses Glu266, implicated in DNA binding (30,31), to within 5 Å of the DNA binding cleft. This helix forms part of domain 1b and is located behind the β-hairpin. Docking of the DNA observed in the reported *Thermotoga maritima* UvrA–DNA structure (3PIH.pdb) into this *M. tuberculosis* UvrA–UvrB dimer assembly, followed by slight bending of the duplex at its 5′ and 3′ ends together with minor re-positioning of the UvrA insertion domains to relieve major steric clashes, results in a configuration where both monomers 'straddle' the T-fluorescein lesions at the interface between the two UvrA monomers (36) (Supplementary Figure S4A). These relatively straightforward re-arrangements, which have been implicated in formation of the $UvrA_2B_2$–DNA complex by several groups (17,35,37), result in the creation of favourable contacts between residues within the 257–277 helix and phosphodiester groups comprising the major grooves of the duplex directly adjacent to each lesion. It can therefore be envisaged that conformational changes induced by ATP hydrolysis, either by UvrA or UvrB in this configuration, could result in further DNA distortion and β-hairpin opening for the handover of DNA to each monomer respectively for lesion engagement.

Given the indication from our modeling studies and proposals of other groups that both UvrB monomers are able to interact with a damaged duplex following handover, we next embarked on constructing a possible model of a $UvrB_2$–DNA complex using the available co-ordinates of the UvrB–stem loop complex. This was achieved by applying the operator relating the monomers in our complex to the stem loop structure co-ordinates. In this dimeric configuration, the damaged and

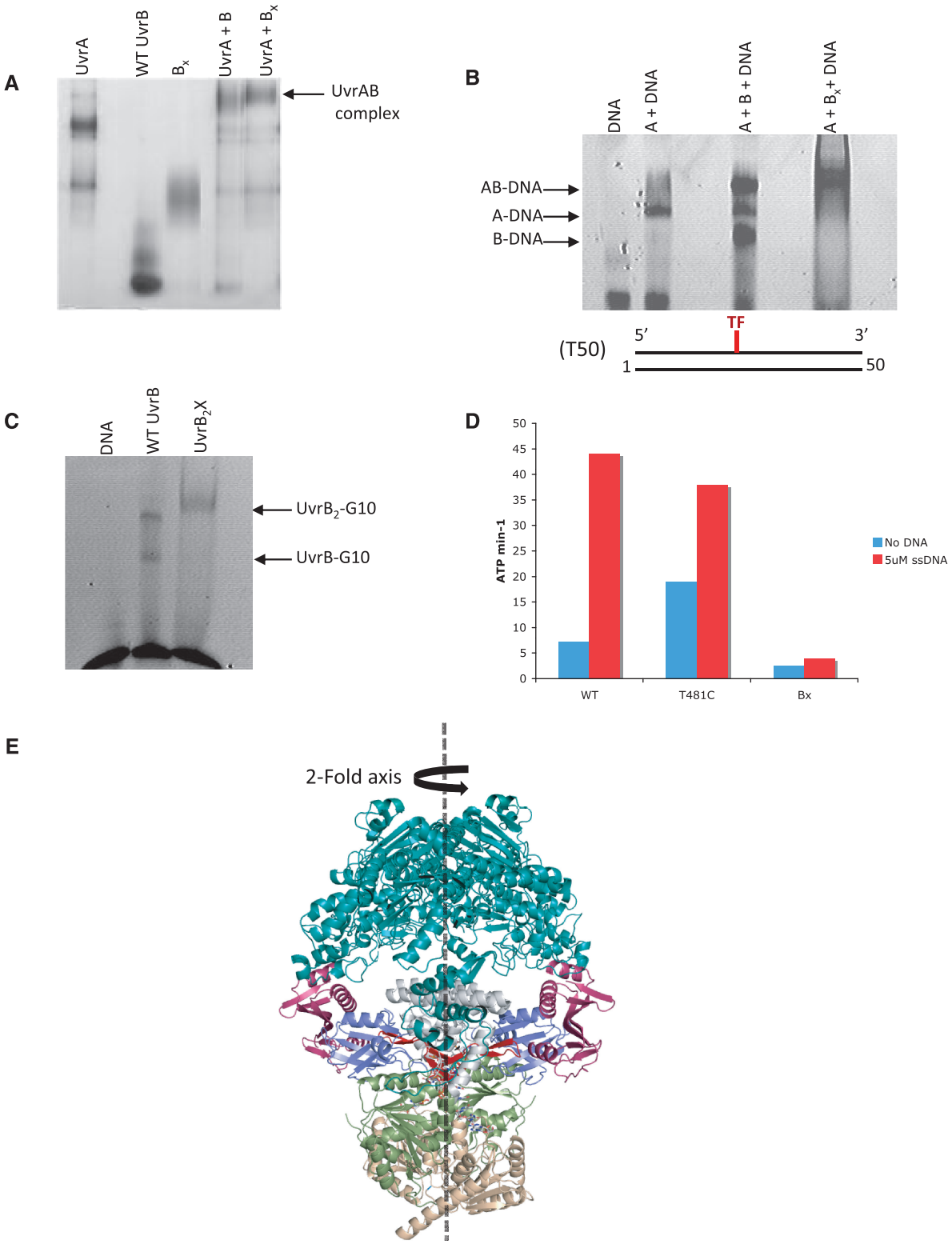

Figure 6. (**A**) A native PAGE gel demonstrating that both UvrB and $UvrB_2X$ form dimeric complexes with UvrA that co-elute. (**B**) UvrA–UvrB ($UvrB_2X$) gel shift assay using the T50 substrate. The UvrA–$UvrB_2X$ complex remains trapped on the DNA unlike wild-type UvrB where a UvrB–DNA complex is formed. (**C**) Gel shift assay illustrating that $UvrB_2X$ is not defective in its ability to associate with DNA. (**D**) ATP-ase assay of $UvrB_2X$ in the presence and absence of DNA. Although $UvrB_2X$ has residual ATP-ase activity, it is no longer stimulated by ssDNA which is the most likely cause of the handover defect. (**E**) Putative model of a $UvrA_2B_{dimer}$ complex. The UvrB dimer can be successfully docked against UvrA with the UvrB interacting domains rotated by 30° relative to their positions in the *B. stearothermophilus* and *T. maritima* structures. In this configuration, the UvrA and UvrB dimer 2-fold axes are aligned and the β-hairpin positioned close to the UvrA dimer interface, the location of the DNA binding site.

non-damaged strands can be simultaneously bound by each of the two β-hairpins having the correct UvrB 5′–3′ strand displacement polarity (Figure 7A) consistent with lesion scanning/detection occurring in both strands. Interestingly, in order for the DNA to be favourably accommodated in the dimer interface, the DNA would have to be kinked (through ~90°) and substantially unpaired in the vicinity of both β-hairpins. Based on this distorted duplex, approximately 20–24 nt in each strand (taking into account the additional protein–DNA contacts observed in our structure) would interact directly with the UvrB dimer. This is consistent both with early electron microscopy (EM) (38) and more recent atomic force microscopy (AFM) (16) studies that demonstrate severe distortion of the DNA in the UvrB–DNA complex together with the reported DNase I footprint of ~24 nt (39). Interestingly, our model also places Tyr95, an important residue implicated in DNA binding, within the unpaired region of the duplex where it intercalates favourably with the disrupted bases as proposed (40). In order to accommodate this partially denatured duplex, many of the protein–protein interactions observed at the N-terminus of the dimer in our crystal structure would thus have to be substituted for protein–DNA contacts in keeping with the inability of $UvrB_2X$ to support handover.

Site-directed mutagenesis reveals a dual function for domain 2 of UvrB

The apparent co-localization of groups shown to be either important or essential for handover together with the ability to generate models of putative $UvrA_2B_2$–DNA and $UvrB_2$–DNA complexes, prompted us to investigate the extent to which residues located in the dimer interface contribute to stabilization of these intermediates. We therefore generated a series of double and single mutants designed to disrupt key protein–protein interactions at its N- and C-termini that were subsequently analysed using gel shift assays. An R194E/D187R double mutant was produced to target the β-hairpin/domain 2 interactions, an R489P single mutant to investigate the effects of disrupting the C-terminal helix in domain 3 and an R194E/I485E double mutant to ascertain the effects of targeting both regions. All mutants were found to be folded as judged by their ability to form the $UvrA_2B_2$ complex with wild-type affinity (Supplementary Figure S4B), but interestingly, gave very different results with respect to handover and formation of the UvrB–DNA complex. As might be expected, the R489P mutant was the most defective (Figure 7B). This substitution resulted in loss of DNA binding activity when incubated with the G10 substrate and an inability to form the UvrA mediated UvrB–T50 DNA complex. Disruption of the domain 3 helix is likely to impact on the protein–DNA interactions mediated by Arg506 which also contacts the carbonyl oxygen of Ser477, five residues upstream of Thr481 (see 'Overall dimer structure, DNA and ATP binding sites' section). A similar but milder phenotype was also observed for the R194E/I485E double mutant, that although defective in DNA binding could nonetheless form a UvrB–DNA complex in the presence of UvrA (Figure 7C). Quite unexpectedly, the R194E/D187R mutant demonstrated enhanced DNA binding activity relative to wild-type UvrB when self and UvrA loaded onto the G10 and T50 substrates, respectively. Although these results on aggregate indicate that Arg194 does not appreciably contribute to stabilization of either the $UvrA_2B_2$–DNA or $UvrB_2$–DNA complexes, our model of a putative $UvrB_2$–DNA complex positions Asp187, Arg189 (Gln189 in *B. subtilis* UvrB) and Arg190 (a strictly conserved residue also located in the dimer interface but disordered from cβ in both monomers) to within 4 Å of the melted duplex in the interfacial region between the two UvrB monomers (Figure 7D). The effects of the D187R substitution could therefore be explained by arginine mediating direct interactions with the phosphodiester backbone.

To establish whether domain 2 does indeed also function as a DNA binding element, Q189A and R190E single mutants were generated and subsequently analysed. While Q189A gave similar results to wild-type UvrB, R190E was significantly diminished in its capacity to bind DNA as predicted by our model (Figure 7E). This almost complete abolition of DNA binding activity evident with the G10 substrate was partially rescued by UvrA although the resulting $UvrB_2$–DNA complex was significantly reduced compared to that obtained with wild-type UvrB. Our results for the first time illustrate the importance of the domain 3 helix in handover and formation of the $UvrB_2$–DNA complex while also revealing that domain 2 has an essential role in stabilizing these important complexes.

DISCUSSION

We present the first crystal structure of a UvrB dimer in complex with ssDNA and AMPPCP that we have shown to be biologically relevant. While the nature of this dimer and its relevance to the UvrABC pathway could only be speculated, our studies have revealed its configuration where the dimer interface comprises elements from the β-hairpin, domain2 and a highly conserved helix (spanning residues 481–495) within domain 3. We have shown that this dimer proficiently interacts with DNA and UvrA which lead us to construct a putative model of a $UvrA_2B_2$–DNA damage engagement complex. A simple rotation of the UvrA UvrB binding domains through ~30° resulted in a more favourable configuration for DNA handover in which the helix spanning residues 257–277 in domain 1b, implicated in DNA binding and located directly behind the β-hairpin, were brought into close proximity with the UvrA DNA binding region and, in particular, the lesion site in both monomers. This model, in common with previous EM studies, predicts that the DNA would have to undergo considerable deformation (bending and melting) in the vicinity of the lesion for handover.

Our results also revealed that although the domain 3 helix and residues within domain 2 are essential for DNA binding and thus handover and formation of the $UvrB_2$–DNA complex, the dimer interface observed in

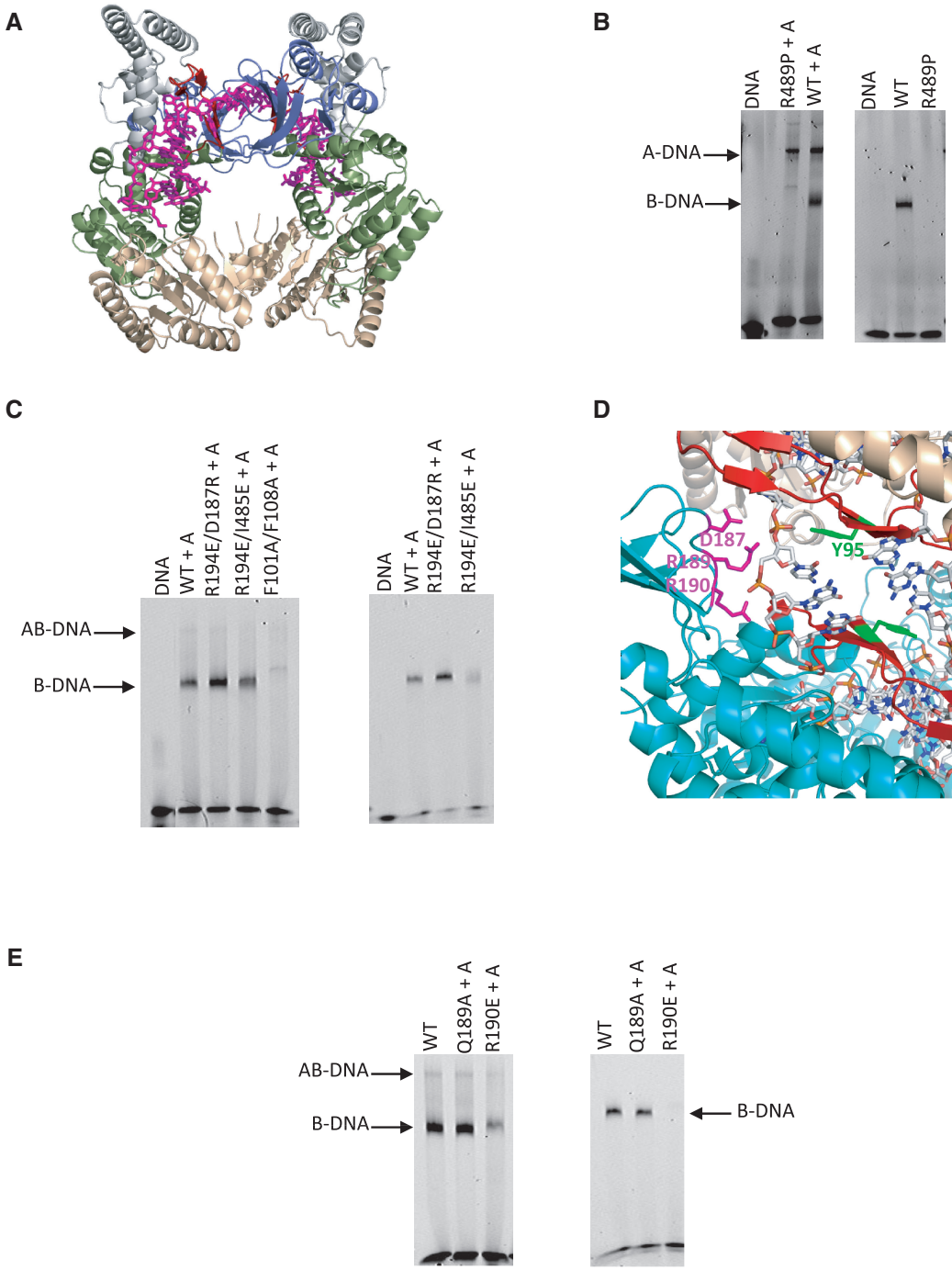

Figure 7. (**A**) A putative $UvrB_2$–DNA complex derived by applying the operator relating the two monomers in our dimer to the UvrB–stem loop DNA monomer co-ordinates (2FDC.pdb). (**B**) Gel shift assays performed with the R489P mutant in the presence of UvrA and the T50 substrate (left) and in the presence of the G10 self-loading substrate (right). In both instances, R489P is entirely defective in its ability to form the B–DNA complex. (**C**) Left: gel shift assays of the R194E/D187R and R194E/I485E interfacial mutants in the presence of UvrA and the T50 substrate (the β-hairpin mutant F101A/F108A is provided as a control since it is entirely defective in its capacity to form a UvrB–DNA complex either in the presence or absence of UvrA). The R194E/D187R mutant exhibits greater affinity for DNA in the UvrB–DNA complex compared to native UvrB while the R194E/I485E has almost wild type affinity. Right: gel shift assays of the same mutants (excluding F101A/F108A) performed using the G10 substrate. The R194E/D187R mutant similarly displays a higher affinity for DNA that contrasts with R194E/I485E that is highly defective. (**D**) The putative $UvrB_2$–DNA model viewed from the interfacial region between the two monomers. Asp187 and Arg190 are both appropriately positioned to interact with the highly distorted duplex. In the model, Tyr95 at the base of the β-hairpin is also predicted to intercalate between the disrupted bases. (**E**) Gel shift assays performed using the R190E mutant in the presence of UvrA and the T50 substrate (left) and in the presence of the G10 substrate (right). In both instances, R190E is defective in its capacity to form the UvrB–DNA complex although there is partial rescue in the presence of UvrA.

our crystal structure is unlikely to support duplex loading and would thus need to be disrupted, based on the inability of $UvrB_2X$ to form this intermediate on the T50 substrate in the presence of UvrA. It would appear that relative motions between the two UvrB monomers are required that are likely to derive from their intrinsic helicase activities that are drastically attenuated in $UvrB_2X$ due to tethering by the cross-linker. Our findings, however, do favour a $UvrA_2B_2$–DNA complex in which the UvrB monomers are (at least initially) similarly orientated to what we observe in our dimer given that $UvrB_2X$ is nonetheless capable of interacting with UvrA and forming both a $UvrA_2B_2$–T50 DNA and a $UvrB_2X$–G10 DNA complex. Although dimerization is not a pre-requisite for the initial binding of UvrB to UvrA, it is notable that both UvrB molecules in the $UvrA_2B_2$ complex structure, despite being separated by 145 Å, are oriented such that domain 2, domain 3 and the β-hairpin that form the interface in our structure are directed inwards towards each other. This relative positioning is likely to give rise to an assembly reminiscent of our dimer in the event that the two monomers are brought together for lesion engagement and handover as suggested (17).

The possibility of each monomer being able to sequester a single, opposing strand behind its β-hairpin in the correct polarity, lead to the construction of a model for the $UvrB_2$–DNA intermediate in which the DNA is doubly kinked in the interfacial region between the two UvrB monomers. This model is in good agreement with DNase I footprinting studies which suggest ~24 nt are in contact with UvrB and is supported by our site directed mutagenesis studies that reveal Arg190 within domain 2 as an important residue in DNA binding. This model also places Tyr95, an important damage detection residue located at the β-hairpin base, within the denatured region of the duplex where it intercalates between the disrupted bases as proposed. In order for these interactions to occur, the protein–protein interactions in our crystal structure would thus need to be abrogated to enable these residues to mediate important contacts with DNA as indicated by the failure of $UvrB_2X$ to form a $UvrB_2X$–T50 DNA complex previously discussed. Interestingly, the configuration of UvrB and DNA in our model also provides an explanation for the DNA 'wrapping' observed in the AFM studies of both the UvrAB–DNA and UvrB–DNA complexes given that protein–DNA interactions involving nucleotides in the 5′ and 3′ strands close to the lesion would result in the duplex being channeled across equivalent faces of the UvrB dimer related by the NCS 2-fold axis (Supplementary Figure S4C). The emergent ends would, as a consequence, be related by angles greater than 90° as observed in the early electron micrographs (38).

Essential to handover and formation of the $UvrB_2$–DNA and pre-incision complexes is the DNA-dependent ATPase activity of UvrB. Although there has yet to be a detailed understanding of how this coupling of ATP hydrolysis and DNA binding is facilitated for these stages in the repair process, insights have been provided by the domain 3–DNA interactions centred on Arg506. Arg506, an important residue in DNA binding, is connected via a network of salt bridges and hydrogen bonds involving residues Arg540 and Asp510 to Arg543 an essential ATP binding residue. Interestingly, there is a lack of extensive protein–DNA contacts mediated by domain 3 and no evidence of the substantial domain 1a domain 3 movements observed in equivalent domains of the other SF1/SF2 helicases. This may be a reflection of UvrB being mechanistically distinct as a consequence of having only a limited helicase activity. Our results may therefore suggest that once handover has occurred, the lesion is approximately in the correct position for formation of the pre-incision complex as proposed by Gordienko *et al.* (41) (see below). Thus, subsequent cycles of ATP binding and hydrolysis may function to modulate the domain 3–DNA interactions involving Arg506 and Glu478 in order to manipulate the duplex into an appropriate conformation for recognition and incision by UvrC. Our hypothesis is supported by mutagenesis studies involving an E478A mutant that although capable of producing a UvrB–DNA complex, was defective in incision (30,31). Our structure also reveals that T7 associated with monomer A undergoes base flipping. The resultant extra-helical thymine is stabilized by interactions involving Arg123 that is pivotal to damage specific repair. Interestingly, mutation of Arg123 results in attenuated ATPase activity and loss of handover that have been interpreted to suggest that Arg123 binds DNA via an association with the phosphodiester backbone. Our findings reveal that although Arg123 does interact with DNA, the mode of interaction alternatively involves the nucleotide base resulting in the β-hairpin sequestered strand being more tightly bound at the 5′ end as proposed by Moolenaar *et al.* (12). This may be a contributing factor to formation of the pre-incision complex by anchoring and thus locking the position of the DNA prior to further manipulation. Arg123, together with residues Gly147–Gly149 and His248–Val250, may also function to transmit signals to the symmetry related monomer via domain 2 possibly to facilitate dimer dissociation.

Although our studies support a mechanism involving lesion searching in both strands simultaneously in common with those of several groups, the 3′–5′ nature of the UvrB 'helicase' polarity would lead to the buildup of significant torque during the damage probing process. This could be offset either by damage detection being performed in each strand individually as proposed by Verhoeven *et al.* (16) utilizing the intrinsic helicase activity of each UvrB monomer for translocation to the lesion site suggested by Jeruzalmi (17) and others or by UvrA positioning the UvrB monomers in close proximity to potential lesions most likely in response to conformational changes induced by ATP hydrolysis. In the latter case, lesion engagement would thus require only a small number of limited translocation or probing cycles consistent with our model of the $UvrA_2B_2X$–DNA complex, where the UvrB monomers are more centrally located with respect to the putative lesion site than in the $UvrA_2B_2$ complex. This is supported by the observation that UvrA has a preference for DNA duplexes containing damage and a defined DNase I footprint of ~32 nt.

The $UvrA_2B_2$ 'helicase' additionally exhibits poor strand displacement activity (restricted to a maximum of ~27 nt) that might alternatively be a by-product of the conformational changes required for a more limited lesion probing process (41). It is interesting to speculate, however, that torque may have an important role in dissociation of the $UvrA_2B_2$–DNA complex in the event that a lesion is detected by one monomer or in situations where they fail to be identified.

While our studies have revealed the nature of the UvrB dimer that contains elements mimetic of the handover and $UvrB_2$–DNA intermediates, and provided insights into the configurations and functioning of these complexes, many issues remain unresolved. Included amongst them is the molecular basis underlying handover and the exact nature of the pre-incision complex. Pivotal to addressing these important issues are crystal structures of $UvrA_2B_2$–DNA complexes at different stages of the handover process.

ACCESSION NUMBERS

3V4R.

SUPPLEMENTARY DATA

Supplementary Data are available at NAR Online: Supplementary Figures 1–4.

ACKNOWLEDGEMENTS

We would like to thank Dr Timothy Waters for his contributions at the early stages of the project.

FUNDING

In house funds from UCL/Birkbeck; Biotechnology and Biological Sciences Research council Doctoral Training Grant (to M.P.J.W.). Funding for open access charge: In house funds from UCL/Birkbeck.

Conflict of interest statement. None declared.

REFERENCES

1. Van Houten,B., Croteau,D.L., DellaVecchia,M.J., Wang,H. and Kisker,C. (2005) 'Close-fitting sleeves': DNA damage recognition by the UvrABC nuclease system. *Mutat. Res.*, **577**, 92–117.
2. Truglio,J.J., Croteau,D.L., Van Houten,B. and Kisker,C. (2006) Prokaryotic nucleotide excision repair: the UvrABC system. *Chem. Rev.*, **106**, 233–252.
3. Friedberg,E.C., Walker,G.C. and Siede,W. (1995) *DNA Repair and Mutagenesis*. ASM Press, Washington DC.
4. Seeley,T.W. and Grossman,L. (1989) Mutations in the *Escherichia coli* UvrB ATPase motif compromise excision repair capacity. *Proc. Natl Acad. Sci. USA*, **86**, 6577–6581.
5. Verhoeven,E.E., Wyman,C., Moolenaar,G.F., Hoeijmakers,J.H. and Goosen,N. (2001) Architecture of nucleotide excision repair complexes: DNA is wrapped by UvrB before and after damage recognition. *EMBO J.*, **20**, 601–611.
6. Wang,H., Lu,M., Tang,M.S., Van Houten,B., Ross,J.B., Weinfeld,M. and Le,X.C. (2009) DNA wrapping is required for DNA damage recognition in the *Escherichia coli* DNA nucleotide excision repair pathway. *Proc. Natl Acad. Sci. USA*, **106**, 12849–12854.
7. Moolenaar,G.F., Franken,K.L., van de Putte,P. and Goosen,N. (1997) Function of the homologous regions of the *Escherichia coli* DNA excision repair proteins UvrB and UvrC in stabilization of the UvrBC-DNA complex and in 3′-incision. *Mutat. Res.*, **385**, 195–203.
8. Hildebrand,E.L. and Grossman,L. (1999) Oligomerization of the UvrB nucleotide excision repair protein of *Escherichia coli*. *J. Biol. Chem.*, **274**, 27885–27890.
9. Verhoeven,E.E., van Kesteren,M., Turner,J.J., van der Marel,G.A., van Boom,J.H., Moolenaar,G.F. and Goosen,N. (2002) The C-terminal region of *Escherichia coli* UvrC contributes to the flexibility of the UvrABC nucleotide excision repair system. *Nucleic Acids Res.*, **30**, 2492–2500.
10. Caron,P.R., Kushner,S.R. and Grossman,L. (1985) Involvement of helicase II (uvrD gene product) and DNA polymerase I in excision mediated by the uvrABC protein complex. *Proc. Natl Acad. Sci. USA*, **82**, 4925–4929.
11. Husain,I., Van Houten,B., Thomas,D.C., Abdel-Monem,M. and Sancar,A. (1985) Effect of DNA polymerase I and DNA helicase II on the turnover rate of UvrABC excision nuclease. *Proc. Natl Acad. Sci. USA*, **82**, 6774–6778.
12. Moolenaar,G.F., Schut,M. and Goosen,N. (2005) Binding of the UvrB dimer to non-damaged and damaged DNA: residues Y92 and Y93 influence the stability of both subunits. *DNA Repair (Amst)*, **4**, 699–713.
13. Pakotiprapha,D., Liu,Y., Verdine,G.L. and Jeruzalmi,D. (2009) A structural model for the damage-sensing complex in bacterial nucleotide excision repair. *J. Biol. Chem.*, **284**, 12837–12844.
14. DellaVecchia,M.J., Merritt,W.K., Peng,Y., Kirby,T.W., DeRose,E.F., Mueller,G.A., Van Houten,B. and London,R.E. (2007) NMR analysis of [methyl-13C]methionine UvrB from Bacillus caldotenax reveals UvrB-domain 4 heterodimer formation in solution. *J. Mol. Biol.*, **373**, 282–295.
15. Malta,E., Moolenaar,G.F. and Goosen,N. (2007) Dynamics of the UvrABC nucleotide excision repair proteins analyzed by fluorescence resonance energy transfer. *Biochemistry*, **46**, 9080–9088.
16. Verhoeven,E.E., Wyman,C., Moolenaar,G.F. and Goosen,N. (2002) The presence of two UvrB subunits in the UvrAB complex ensures damage detection in both DNA strands. *EMBO J.*, **21**, 4196–4205.
17. Pakotiprapha,D., Samuels,M., Shen,K., Hu,J.H. and Jeruzalmi,D. (2012) Structure and mechanism of the UvrA-UvrB DNA damage sensor. *Nat. Struct. Mol. Biol.*, **19**, 291–298.
18. Eryilmaz,J., Ceschini,S., Ryan,J., Geddes,S., Waters,T.R. and Barrett,T.E. (2006) Structural insights into the cryptic DNA-dependent ATPase activity of UvrB. *J. Mol. Biol.*, **357**, 62–72.
19. Pannier,M., Veit,S., Godt,A., Jeschke,G. and Spiess,H.W. (2000) Dead-time free measurement of dipole-dipole interactions between electron spins. *J. Magn. Reson.*, **142**, 331–340.
20. Jeschke,G., Chechik,V., Ionita,P., Godt,A., Zimmermann,H., Banham,J., Timmel,C.R., Hilger,D. and Jung,H. (2006) A comprehensive software package for analyzing pulsed ELDOR data. *Appl. Magn. Reson.*, **30**, 473–498.
21. Kabsch,W. (2010) Xds. *Acta Crystallogr. D Biol. Crystallogr.*, **66**, 125–132.
22. Kabsch,W. (2010) Integration, scaling, space-group assignment and post-refinement. *Acta Crystallogr. D Biol. Crystallogr.*, **66**, 133–144.
23. Collaborative Computational Project Number 4. (1994) The CCP4 suite: programs for protein crystallography. *Acta Crystallogr. D Biol. Crystallogr.*, **50**, 760–763.
24. Emsley,P. and Cowtan,K. (2004) Coot: model-building tools for molecular graphics. *Acta Crystallogr. D Biol. Crystallogr.*, **60**, 2126–2132.
25. Adams,P.D., Grosse-Kunstleve,R.W., Hung,L.W., Ioerger,T.R., McCoy,A.J., Moriarty,N.W., Read,R.J., Sacchettini,J.C., Sauter,N.K. and Terwilliger,T.C. (2002) PHENIX: building new software for automated crystallographic structure determination. *Acta Crystallogr. D Biol. Crystallogr.*, **58**, 1948–1954.
26. Bricogne,G., Blanc,E., Brandl,M., Flensburg,C., Keller,P., Paciorek,W., Roversi,P., Sharff,A., Smart,O.S., Vonrhein,C. *et al.* (2011) *Buster*. Global Phasing Ltd., Cambridge, UK.

27. Chen,V.B., Arendall,W.B. 3rd, Headd,J.J., Keedy,D.A., Immormino,R.M., Kapral,G.J., Murray,L.W., Richardson,J.S. and Richardson,D.C. (2010) MolProbity: all-atom structure validation for macromolecular crystallography. *Acta Crystallogr D Biol Crystallogr*, **66(Pt 1)**, 12–21.
28. Fairman-Williams,M.E., Guenther,U.P. and Jankowsky,E. (2010) SF1 and SF2 helicases: family matters. *Curr. Opin. Struct. Biol.*, **20**, 313–324.
29. Bienstock,R.J., Skorvaga,M., Mandavilli,B.S. and Van Houten,B. (2003) Structural and functional characterization of the human DNA repair helicase XPD by comparative molecular modeling and site-directed mutagenesis of the bacterial repair protein UvrB. *J. Biol. Chem.*, **278**, 5309–5316.
30. Lin,J.J., Phillips,A.M., Hearst,J.E. and Sancar,A. (1992) Active site of (A)BC excinuclease. II. Binding, bending, and catalysis mutants of UvrB reveal a direct role in 3′ and an indirect role in 5′ incision. *J. Biol. Chem.*, **267**, 17693–17700.
31. Hsu,D.S., Kim,S.T., Sun,Q. and Sancar,A. (1995) Structure and function of the UvrB protein. *J. Biol. Chem.*, **270**, 8319–8327.
32. Moolenaar,G.F., Visse,R., Ortiz-Buysse,M., Goosen,N. and van de Putte,P. (1994) Helicase motifs V and VI of the Escherichia coli UvrB protein of the UvrABC endonuclease are essential for the formation of the preincision complex. *J. Mol. Biol.*, **240**, 294–307.
33. Skorvaga,M., DellaVecchia,M.J., Croteau,D.L., Theis,K., Truglio,J.J., Mandavilli,B.S., Kisker,C. and Van Houten,B. (2004) Identification of residues within UvrB that are important for efficient DNA binding and damage processing. *J. Biol. Chem.*, **279**, 51574–51580.
34. Wang,H., DellaVecchia,M.J., Skorvaga,M., Croteau,D.L., Erie,D.A. and Van Houten,B. (2006) UvrB domain 4, an autoinhibitory gate for regulation of DNA binding and ATPase activity. *J. Biol. Chem.*, **281**, 15227–15237.
35. Rossi,F., Khanduja,J.S., Bortoluzzi,A., Houghton,J., Sander,P., Guthlein,C., Davis,E.O., Springer,B., Bottger,E.C., Relini,A. *et al.* (2011) The biological and structural characterization of *Mycobacterium tuberculosis* UvrA provides novel insights into its mechanism of action. *Nucleic Acids Res.*, **39**, 7316–28.
36. Jaciuk,M., Nowak,E., Skowronek,K., Tanska,A. and Nowotny,M. (2011) Structure of UvrA nucleotide excision repair protein in complex with modified DNA. *Nat. Struct. Mol. Biol.*, **18**, 191–197.
37. Timmins,J., Gordon,E., Caria,S., Leonard,G., Acajjaoui,S., Kuo,M.S., Monchois,V. and McSweeney,S. (2009) Structural and mutational analyses of *Deinococcus radiodurans* UvrA2 provide insight into DNA binding and damage recognition by UvrAs. *Structure*, **17**, 547–558.
38. Shi,Q., Thresher,R., Sancar,A. and Griffith,J. (1992) Electron microscopic study of (A)BC excinuclease. DNA is sharply bent in the UvrB-DNA complex. *J. Mol. Biol.*, **226**, 425–432.
39. Zou,Y., Liu,T.M., Geacintov,N.E. and Van Houten,B. (1995) Interaction of the UvrABC nuclease system with a DNA duplex containing a single stereoisomer of dG-(+)- or dG-(-)-anti-BPDE. *Biochemistry*, **34**, 13582–13593.
40. Zou,Y., Ma,H., Minko,I.G., Shell,S.M., Yang,Z., Qu,Y., Xu,Y., Geacintov,N.E. and Lloyd,R.S. (2004) DNA damage recognition of mutated forms of UvrB proteins in nucleotide excision repair. *Biochemistry*, **43**, 4196–4205.
41. Gordienko,I. and Rupp,W.D. (1997) The limited strand-separating activity of the UvrAB protein complex and its role in the recognition of DNA damage. *EMBO J.*, **16**, 889–895.